Materials Physics and Mechanics. 2022;50(3): 509-517
Research article
http://dx.doi.org/10.18149/MPM.5032022_13

Submitted: July 8, 2022
Approved: September 13, 2022
Accepted: October 7, 2022

Impact of forced cooling of the joint zone and thermal effect on the distribution values of residual stress generated by arc welding

A.V. Tkacheva✉, E.E. Abashkin

Institute of Machinery and Metallurgy of the Far Eastern Branch of the Russian Academy of Sciences, 1, Metallurgov st., Komsomolsk-na-Amure, 681005, Russia

✉ 4nansi4@mail.ru

Abstract. The search for technological options to obtain strong units with small deformation values determines the study of the local thermal effect on the distribution of residual stresses in permanent joints of metal structures made by arc welding with forced cooling. The mathematical model is based on the Prandtl-Reiss model in which the Hooke law is replaced by the Duhamel-Neumann law and the Mises criterion is supplemented by the Johnson-Cook strain hardening function. The elastic moduli, as well as the yield strength, are assumed to be temperature-dependent. The calculated values of residual stresses show the positive effect of forced cooling of the welded zone.

Keywords: welding, mathematical model, Johnson-Cook strain hardening function, residual stresses, deformation, heat affected zone

Acknowledgements. *The work was carried out within the state assignment of Khabarovsk Federal Research Center of the Far Eastern Branch of the Russian Academy of Sciences.*

Citation: Tkacheva AV, Abashkin EE. Impact of forced cooling of the joint zone and thermal effect on the distribution values of residual stress generated by arc welding. *Materials Physics and Mechanics*. 2022;50(3): 509-517. DOI: 10.18149/MPM.5032022_13.

1. Introduction.

Welding technology is used extensively in modern industry to produce metal structures. A large part of welded constructions is not only in one-piece and small batch production but also in mass production. This makes it necessary to increase productivity and reduce the cost of all operational cycles. At the same time, products must have improved material performance and physical and mechanical properties.

There are different welding techniques, such as electric arc, plasma, electro slag, electro-beam, induction, laser, and friction welding. Each method has its own advantages and disadvantages. Of the above-mentioned technologies, electrode wire arc welding is the most common and in demand due to its ease of use, mobility of use, and inexpensive consumables [1-4]. Increasing the productivity of arc welding requires an increase in speed, which in turn increases the thermal capacity of the arc flow. This negatively affects the strength properties of permanent joints. One of the ways to solve this problem is seen in the additional removal of heat from the zone of local thermal impact. The need for forced cooling of the weld metal and the heat-affected zone of the welded joint occurs when welding materials are with high sensitivity to high-temperature heating. Such as high-chromium ferritic steels and single-phase iron-chromium-aluminium alloys, as well as materials whose properties are determined

by the degree of dispersion of the precipitated phases, which, in turn, depends on the cooling rate of the crystallizing metal [5-14].

However, due to a significant number of factors affecting the formation of the weld metal and the heat-affected zone (HAZ), predicting the result of heat-affected zone cooling on the strength and deformation characteristics of the welded joint becomes very difficult.

It has been established that the material of the part should be considered elastoplastic, as only in this case there is a possibility of quantitative and qualitative estimation of processes of formation of residual stress fields in the near-weld zone, which influence the quality of joint is mainly negative. [15].

Elastic and plastic properties are temperature dependent, so the main difficulty is in iterative tracking the nucleation and disappearance of plastic flow zones. Plastic flow generates irreversible deformations which then form residual stresses during unloading and cooling. Since all coefficients depend on temperature, it is not possible to find a solution analytically. Despite a considerable number of theoretical and experimental studies on the prediction of the final properties of the resulting permanent joint, the processes of forced cooling of the welding zone, which determine the behaviour of the material under these conditions, are poorly studied at present.

Welding technology is being modernised both experimentally [16-19] and theoretically using a mathematical apparatus [20-23].

Mathematical modeling of the process of electric arc welding with forced cooling, taking into account the geometric parameters and thermophysical properties of the heat removal, makes it possible to optimise this technology without resorting to long and expensive experiments. It is enough to build a correct mathematical model once based on the mechanical behavior of the object under study in order to further analyze the influence of various thermophysical factors.

This work is aimed at obtaining a mathematical model of the evolution of thermal stresses in the near-weld zone and calculating the thermomechanical parameters of the process, taking into account the dependences of the yield strength, elastic models, and the hardening coefficient of resistance to plastic flow on temperature, including the calculation of their final values and the distribution of residual stresses. The aim of the work is to determine the effect of forced cooling on the level and distribution of residual stresses in the area of the weld.

2. Materials and Methods

Temperature studies of the welding area. Process modeling is shown in Fig. 1. The plates 3 mm thick, made from mild steel, are joined using an electric arc welding at a speed V. Behind there is a curvilinear horseshoe-shaped heat removal, which reduces the temperature in the HAZ. After cooling, the connection of the plates becomes inseparable. Now it is necessary to calculate the residual stresses in the connection zone and the HAZ. We divide the problem into two: temperature and mechanical and solve them in this sequence.

In arc welding, the process of heat distribution in a solid body is described by a nonlinear differential thermal conductivity equation, taking into account the active heat source:

$$c(T)\rho(T)\frac{\partial T}{\partial t} = div(\lambda(T)gradT) + q, \quad (1)$$

where $\lambda(T)$ – thermal conductivity $Wt/(m^{\circ}\mathrm{C})$, $c(T)$ – thermal capacity $J/(kg^{\circ}\mathrm{C})$, $\rho(T)$ – density kg/m^3, q – volumetric power density of the heat source Wt/m^3.

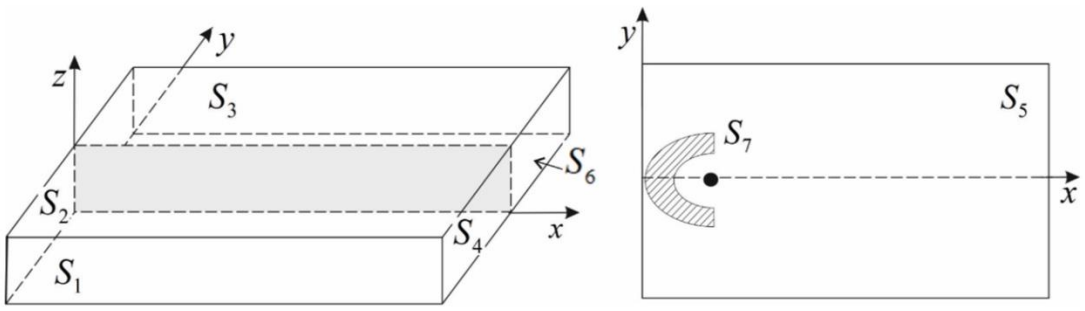

Fig. 1. Problem diagram

The heat source is modelled by the well-known ellipsoid proposed by John A. Goldak [24]. Figure 2 shows the shape of the heat flux in platinum during welding.

$$q_s = f_s \frac{6\sqrt{3Q}}{a_s bc\pi^{1.5}} e^{-3\left(\left(\frac{x+v(\tau-t)}{a_s}\right)^2+\left(\frac{y}{b}\right)^2+\left(\frac{z}{c}\right)^2\right)};\ q_l = f_l \frac{6\sqrt{3Q}}{a_l bc\pi^{1.5}} e^{-3\left(\left(\frac{x+v(\tau-t)}{a_l}\right)^2+\left(\frac{y}{b}\right)^2+\left(\frac{z}{c}\right)^2\right)}, \quad (2)$$

where Q – effective thermal capacity of the heating source (for arc welding Q = η·I·U, Wt), τ – time elapsed since the start of the source, sec; t – current time, sec; v – travel rate of the heating source (welding rate), m/sec; x, y, z – ellipsoid semi-axes in the coordinate directions OX, OY, OZ, m; f_s and f_l – coefficients defining the ratios for the heat input to the front and back of the ellipsoid; a_s, a_l, b, c – the corresponding radii of the normal distribution, m.

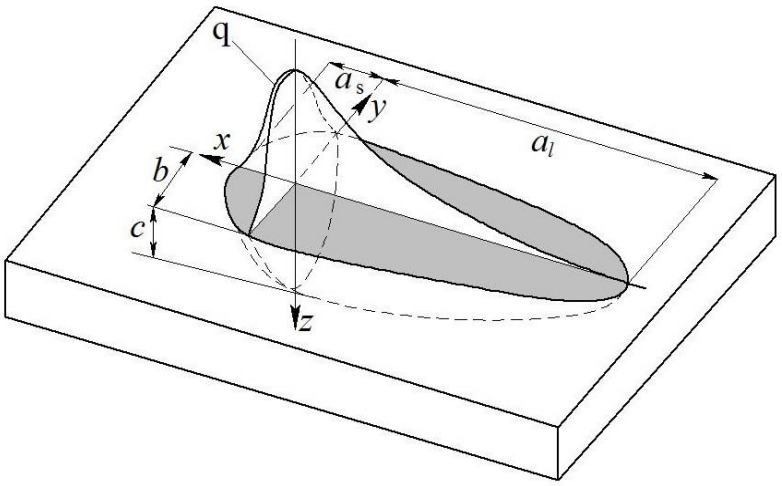

Fig. 2. Heating source diagram

Based on the above, there is the following relationship between the coefficients f_s and f_l: $f_s = \frac{2a_s}{a_s + a_l}$; $f_l = \frac{2a_s}{a_s + a_l}$; $f_s + f_l = 2$.

On the surface free from heat removal and the heat source, the boundary conditions are given by

$$S_1\ -\lambda\frac{\partial T}{\partial y} = \kappa(T - T_0)\ \ S_2\ -\lambda\frac{\partial T}{\partial x} = \kappa(T - T_0);\ S_3\ \lambda\frac{\partial T}{\partial y} = \kappa(T - T_0)\ \ S_4\ -\lambda\frac{\partial T}{\partial x} = \kappa(T - T_0)$$

$$S_5\ -\lambda\frac{\partial T}{\partial z} = \kappa(T - T_0)\ \ S_6\ \lambda\frac{\partial T}{\partial z} = \kappa(T - T_0),\ T_0 = 20\ ^\circ\text{C}.$$

In the cooling area depicted as a horseshoe S_7 (Fig. 1) the boundary conditions are the following: $\lambda\dfrac{\partial T}{\partial z}=-q$.

Mechanical study. It is assumed that at first there are no irreversible deformations in the plate. The deformations are assumed to be small d_{ij} and combined reversible e_{ij} and irreversible p_{ij}.

$$d_{ij}=0.5\left(u_{i,j}+u_{j,i}\right)=e_{ij}+p_{ij} \tag{3}$$

Stresses, elastic deformation, and temperature are connected by the Duhamel-Neumann relation

$$\sigma_{ij}=\left(\lambda e_{kk}-3\alpha K\left(T-T_0\right)\right)\delta_{ij}+2\mu e_{ij}, \tag{4}$$

where λ, μ, $K=\dfrac{2}{3}\mu+\lambda$ elastic moduli, α – linear expansion coefficient.

At high temperatures, the elastic moduli depend on temperature, which is confirmed experimentally [25-32]. For our case, we use their linear dependence.

$$\begin{gathered}E\left(x,y,z,t\right)=E_p-\left(E_p-E_0\right)\theta\left(x,y,z,t\right),\\ v\left(x,y,z,t\right)=0.5-\left(0.5-v_0\right)\theta\left(x,y,z,t\right),\\ \mu=\frac{E}{2\left(1+v\right)},\ \lambda=\frac{vE}{\left(1+v\right)\left(1-2v\right)},\\ \theta=\left(T_p-T\right)\left(T_p-T_0\right)^{-1}.\end{gathered} \tag{5}$$

In (5) E_0 – Young's Modulus at room temperature T_0, E_p – at melting temperature T_p, v_0 – Poisson's ratio at room temperature. After the beginning of the cooling process due to phase solid-state transformations, the elastic moduli v_0 fix their values $E_0'(x)$ and $v_0'(x)$, by this we simulate phase transitions.

Irreversible deformations begin to increase when the stress state reaches the loading surface $f\left(\sigma_{ij},\sigma\right)$ in the stress space, where σ – strain hardening function. Write down the associated plastic flow rule

$$\varepsilon_{ij}^p=dp_{ij}=d\varphi\frac{\partial f\left(\sigma_{ij},\eta\right)}{\partial\sigma_{ij}};\ d\varphi>0. \tag{6}$$

As the loading surface, we take the Mises plastic flow condition, in the left part of which we write the Johnson-Cook strain hardening function [34]

$$\sqrt{\frac{3}{8}\tau_{ij}\tau_{ij}}=\left(A+B\left(\varepsilon^p\right)^n\right)\cdot\left(1+C\,ln\frac{\dot{\varepsilon}^p}{\dot{\varepsilon}_0^p}\right)\theta, \tag{7}$$

where A, B, C, n – material parameters which are found by selection from experimental curves, ε^p – intensity of plastic deformation, $\dot{\varepsilon}^p$ – rate intensity of plastic deformation, $\dot{\varepsilon}_0^p$ – initial rate intensity of deformation, $\dot{\varepsilon}_0^p=0.0006$ 1/sec.

The equilibrium equation supplements the system of equations (3,4,6,7)

$$\sigma_{ij,j}=0. \tag{8}$$

The boundary conditions simulate the free surface; as the initial conditions of the mechanical problem, we take the temperature of the plate in a free state equal to room temperature $T_0=20$ °C. Young's Modulus at room temperature is $E_0=210$ hPa, $E_p=0.3E_0$

at melting temperature $T_p = 1400\,°C$, Poisson's ratio is 0.27, linear expansion coefficient is 11.1×10^{-6}, and yield strength at room temperature is $k_0 = 260$ MPa.

3. Results and discussion

Consider solving the above-described temperature problem for a steel plate. Dependencies $\lambda(T)$, $c(T)$, $\rho(T)$ are taken from source [33]. Plate thickness is 0.003 m, dimensions are 0.2 m×0.2 m, and thermal spot rate is 45 m/h. The heat source characteristics are $Q = 2.5\times10^7$ W, and the source of cooling is 5% of the electric arc power Q.

Figure 3 shows two cases of temperature propagation in platinum material. In the first case, welding took place without forced heat removal; in the second case, forced heat removal was taken into account.

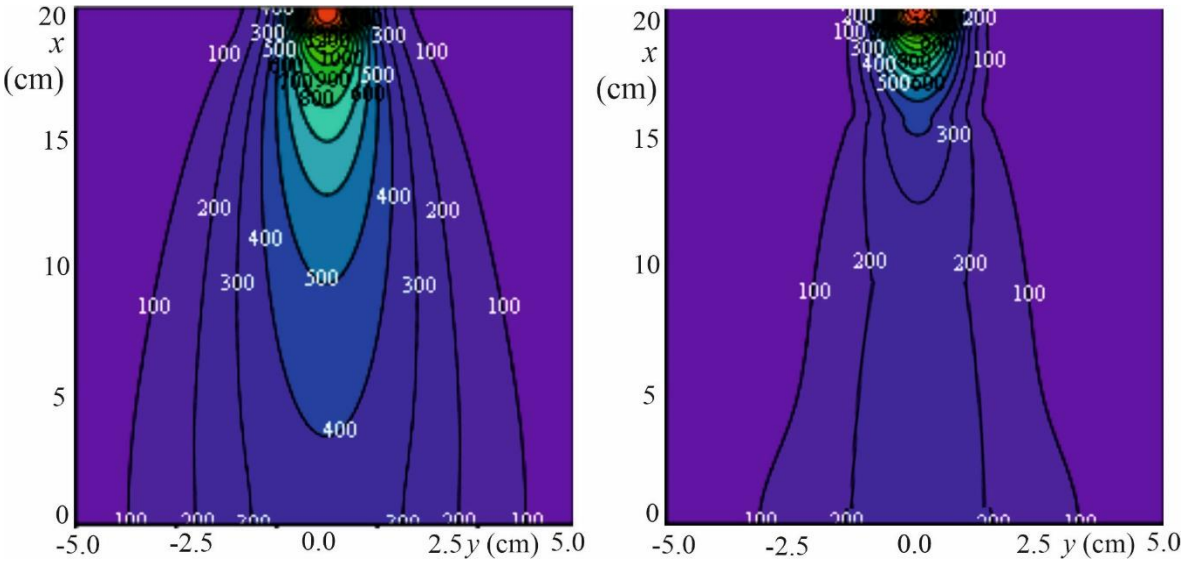

Fig. 3. Temperature distribution within the plate at a distance of 5 cm from the weld at the moment of stopping the welding: a) without cooling; b) with cooling

The data show that the proposed method allows, due to more intensive cooling, to ensure the formation of a narrower weld with a smaller HAZ.

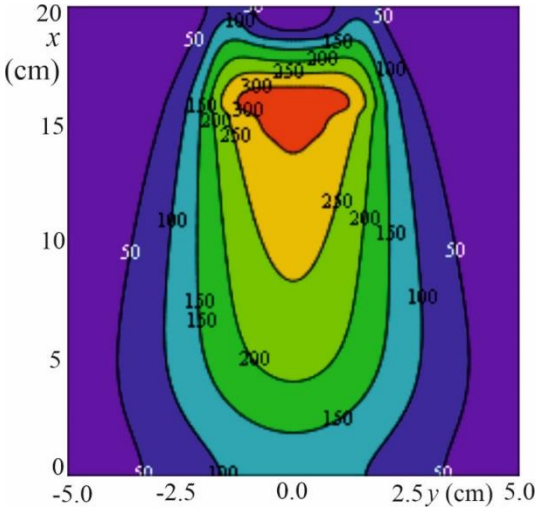

Fig. 4. Temperature difference

The curvilinear shape of the horseshoe-shaped heat removal affects the geometry of the temperature field distribution during welding (Fig. 4), the temperature difference in the weld zone was 300°C.

We solve the problem numerically using the difference method and Newton's iterative method. We use free surface conditions as boundary conditions. For clarity, the distribution of stresses is given on the diagram.

Figure 5 shows the residual stresses generated after the local thermal effect in the plate volume from the center of the weld to the edge of the heat-affected zone. According to the data, during electric arc welding of a thin plate in a butt, residual stresses are formed in the surface layer on the side of the heat source. The tensile stresses are highest in the weld zone and decrease with distance from the weld. Forced cooling reduces the level of residual stresses in comparison with the traditional welding method and reduces the zone of their distribution due to the reduced HAZ.

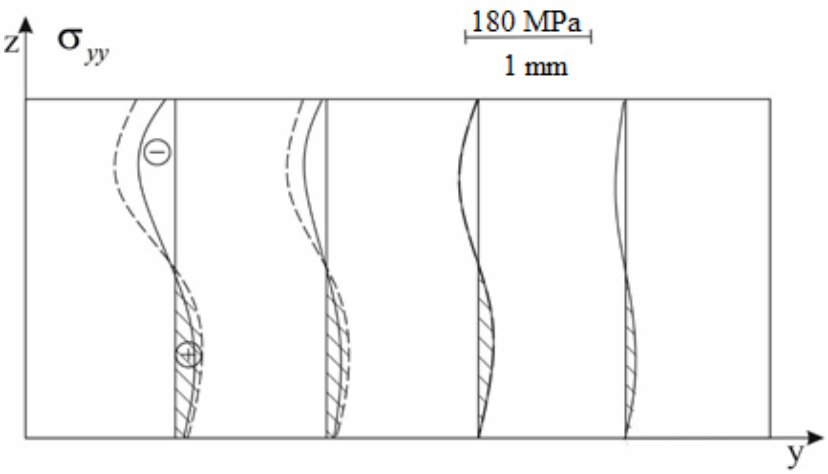

Fig. 5. Stress diagram. The solid line indicates the stress formed in the platinum material with active heat removal, and the dotted line – without it

4. Conclusions

Using small elastoplastic deformations and the Johnson-Cook strain hardening model, the problem of the local thermal effect of movable heat source on a steel plate with active heat removal in the impact area has been solved. The heat removal was 5% of the electric arc power. During its action, residual stresses and the area of their distribution are significantly reduced. This occurs due to a reduction in the time over which irreversible deformations would have grown.

As a result of solving the problem, it has been found that when joining low-carbon steel plates, optimal results are achieved when the welding zone is cooled by a curvilinear heat removal of a horseshoe-shaped configuration with the area of 1336 mm^2 and the speed of electrode movement V = 45 m/h. Forced cooling reduces the level of residual stresses by 28-30% in comparison with the traditional method of welding and reduces the zone of their distribution due to a reduced HAZ by 14%.

Thus, it has been established that the use of electric arc welding with forced cooling will increase the productivity of the process, improving the operational and physical, and mechanical properties of the material.

References

[1] Zhang J, Huang Z, Fang Y, Gu Z, Xie J, Lei J. Experiments and numerical simulations for the mechanical properties of Ni-based superalloys fabricated by laser melting deposition. *Optics & Laser Technology*. 2021;140: 107058.
[2]. Nekrasov R, Galinskii A, Tempel O. Surfacing Technology Materials. *Today Proceedings*. 2019;11: 101-106.
[3]. Wang G, Suder W, Ding J, Williams S. The effect of wire size on high deposition rate wire and plasma arc additive manufacture of Ti-6Al-4V. *Journal of Materials Processing Tech*. 2020. Available from: https://doi.org/10.1016/j.jmatprotec.2020.116842.
[4]. Sokolov NG, Zorin IV, Artemyev AA, Elsukov SC, Fastov SA, Fedosyuk EI, Polunin IA, Mokovozov ND. Surfacing of composite thermo- and wear-resistant alloys using materials containing nanoparticles of refractory chemical compounds. *Proceedings of the Volgograd State Technical University*. 2019;4(227): 61-67.
[5] Vlasov SN, Lapin IE, Savinov AV, Lysak VI, Potapov AN, Atamanyuk VI. *Method of welding in shielding gases with forced cooling of the seam and the heat-affected zone*. RU2232668 (Patent) 2004.
[6] Sołtysiak S. Analysis of structure and material properties in individual zones ofwelded joint. *Journal of Constructional Steel Research.* 2021;187(106978): 290-297.
[7] Zhanga Y, Dinga K, Huob X, Zhaoa B, Fanb B, Zhangb Y, Wanga Y, Weia T, Wua G, Gao Y. Effect of the additional heat input on the microstructure and property in NiCrMoV welded joint simulated by multiple thermal cycles. *Journal of Materials Processing Tech*. 2020;284: 116740.
[8] Yang Y, Pan X. Effect of Mn/N ratio on microstructure and mechanical behavior of simulated welding heat affected zone in 22% Cr lean duplex stainless steel Effect of Mn/N ratio on microstructure and mechanical behavior of simulated welding heat affected zone in 22% Cr lean duplex stainless steel. *Materials Science & Engineering: A*. 2022;835: 142676.
[9] Tao Y, Zhang Z, Xue Z, Ni D, Xiao BL, Ma ZY. Effect of post weld artificial aging and water cooling on microstructure and mechanical properties of friction stir welded 2198-T8 Al-Li joints. *Journal of Materials Science & Technology*. 2022;123: 92-112.
[10] Ebrahimnia M, Malek Ghaini F, Gholizade Sh, Salari M. Effect of cooling rate and powder characteristics on the soundness of heat affected zone in powder welding of ductile cast iron. *Materials and Design*. 2012;33: 551-556.
[11] Echols J, Garrison L, Silva Ch, Lindquist E. Temperature and time effects of post-weld heat treatments on tensile properties and microstructure of Zircaloy-4. *Journal of Nuclear Materials*. 2021;551: 152952.
[12] Lia J, Lia H, Liangc Y, Liuc P, Yanga L, Wanga Y. Effects of heat input and cooling rate during welding on intergranular corrosion behavior of high nitrogen austenitic stainless steel welded joints. *Corrosion Science*. 2020;166: 108445.
[13] Moon J, Lee J, Lee Ch. Reheating cracking susceptibility in the weld heat-affected zone of re duce d activation ferritic-martensitic steels and the effect of Cr content. *Journal of Nuclear Materials.* 2020; 542: 152499.
[14] Kumar S, Natha SK, Kumar V. Continuous cooling transformation behavior in the weld coarse grained heat affected zone and mechanical properties of Nb-microalloyed and HY85 steels. *Materials and Design*. 2016;90: 177-184.
[15] Abashkin EE, Burenin AA, Zhilin SG, Komarov ON, Tkacheva AV. Modeling the distribution of residual stresses in a welded joint. *Physics and mechanics of materials*. 2019;42(5): 671-689.
[16] Becker A, Schroepfer D, Kromm A, Kannengiesser Th. Determination of residual stress evolution during repair welding ofhigh-strength steel components. *Forces in Mechanics.* 2022;6: 100073.

[17] Huaqiang L, Yulong W, Shengdan L, Xiaorong Zh. Effect of cooling conditions on microstructure and mechanical properties of friction stir welded 7055 aluminium alloy joints. *Materials Characterization*. 2018;141: 74-85.
[18] Shojaati M, Bozorg SF, Vatanara M, Yazdizadeh M, Abbasi M. The heat affected zone of X20Cr13 martensitic stainless steel after multiplerepair welding: Microstructure and mechanical properties assessment. *International Journal of Pressure Vessels and Piping*. 2020;188: 104205.
[19] Dak G, Pandey Ch. Experimental investigation on microstructure, mechanical properties, andresidual stresses of dissimilar welded joint of martensitic P92 and AISI 304L austenitic stainless steel. *International Journal of Pressure Vessels and Piping*. 2021;194: 104536.
[20] Farias FWC, Passos AV, Moraes e Oliveira VHP. Microstructural characterization of the physical simulated and welded heat-affected zone of 9% Ni steel pipe. *Journal of materials research and technology*. 2022;17: 3033-3046.
[21] Farias RM, Teixeira PRF, Vilarinho LO. Variable profile heat source models for numerical simulations of arc welding processes. *International Journal of Thermal Sciences*. 2022;179: 107593.
[22] Sun Z, Yu X. Prediction of welding residual stress and distortion in multi-layer butt-welded 22SiMn2TiB steel with LTT filling metal. *Journal of materials research and technology*. 2022;18: 3564-3580.
[23] Afkhami S, Javaheri V, Amraei M, Skriko T, Piili H , Zhao X, Björk T. Thermomechanical simulation of the heat-affected zones in weldedultra-high strength steels: Microstructure and mechanical properties. *Materials & Design.* 2022;213: 110336.
[24] Goldak JA, Akhlagi M. *Computational Welding Mechanics.* U.S.: Springer; 2005.
[25] Cunha Lima RO, Alves Jr C, Alves de Melo AC, Alves SM, Filho L. New technique for deposition and thermochemical treatment of small parts with complex geometry applied to machining inserts. *Journal of materials research and technology*. 2020;9(6): 15811-15823.
[26] Azhar D, Israr E, Kumar A. An investigation on the feasibility of fused deposition modelling process in EDM electrode manufacturing. *CIRP Journal of Manufacturing Science and Technology.* 2019;26: 10-25.
[27] Wang X, Wana J, Wang J, Zhu L, Ruan H. Anomalous sudden drop of temperature-dependent Young's modulus of a plastically deformed duplex stainless steel. *Materials and Design*. 2019;181: 108071.
[28] Xue H, Liu D, Ge R, Pan L, Peng W. The delay loop phenomenon in high temperature elasticity modulus testby in-situ ultrasonic measurements. *Measurement*. 2020;160: 107833.
[29] Latella BA, Humphries SR. Young's modulus of a 2.25 Cr–1Mo steel at elevated temperature. *Scripta Materialia*.2004;51: 635-639.
[30] Lindgren L, Back JG. Elastic properties of ferrite and austenite in low alloy steels versus temperature and alloying. *Material*. 2019;5: 100193.
[31] Rokilan M, Mahendran M. Elevated temperature mechanical properties of cold-rolled steelsheets and cold-formed steel sections. *Journal of Constructional Steel Research*. 2020;167: 105851.
[32] Sung JH, Kim JH, Wagoner RH. A plastic constitutive equation incorporating strain, strain-rate, and temperature. *Int. J. Plast*. 2010;26: 1746-1771.
[33] Kazantsev EI. *Industrial ovens. Reference guide for calculations and design*. Moscow: Metallurgy; 1975.

THE AUTHORS

Tkacheva A.V.
e-mail: 4nansi4@mail.ru
ORCID: 0000-0003-1795-0021

Abashkin E.E.
e-mail: abashkine@mail.ru
ORCID: 0000-0002-9308-1326